almost countable. Ordinary reactions under an effectively low concentration condition are known to produce polymer rings, such as syntheses of cyclic peptides on an oxime resin (*24*). Also, dynamic light scattering yields a diffusion constant of 4×10^{-8} cm^2/s for even very short SWNTs. This value is 10^2 to 10^3 times slower than typical organic molecules in solution. Thus, bimolecular collision is highly suppressed, whereas intramolecular reaction is not affected. This implies that W does not shift to the right during reaction under the present conditions.

Height examinations of the rings in the AFM images show that some rings are thicker than a few nm, implying rings of bundles. Either postaggregation of linear SWNTs onto a single-tube ring or ring closure of a single bundle forms ring-shaped bundles during reaction. It is difficult to verify from AFM images, because the former case may take place also during solvent evaporation. The good fit over the left-hand shoulder of the ring distribution by a single value of p suggests the former case, whereas the fine fit over the right-hand shoulder by the all-tubes distribution of Fig. 3B favors the latter. Unless p depends significantly on a number of individual SWNTs in a bundle, rings can contain both types. For possible controls of the average ring size, it is interesting to see if p depends on the SWNT diameter.

References

1. R. Saito, G. Dresselhaus, M. S. Dresselhaus, *Physical Properties of Carbon Nanotubes* (Imperial College, London, 1998).
2. A. G. Rinzler *et al.*, *Appl. Phys. A* **67**, 29 (1998).
3. W. A. de Heer, A. Châtelain, D. Ugarte, *Science* **270**, 1179 (1995).
4. H. Dai, J. H. Hafner, A. G. Rinzler, D. T. Colbert, R. E. Smalley, *Nature* **384**, 147 (1996).
5. S. S. Wong, E. Joselevich, A. T. Woolley, C. L. Cheung, C. M. Lieber, *Nature* **394**, 52 (1998).
6. P. Kim, C. M. Lieber, *Science* **286**, 2148 (1999).
7. T. Rueckes *et al.*, *Science* **289**, 94 (2000).
8. J. Kong *et al.*, *Science* **287**, 622 (2000).
9. B. Vigolo *et al.*, *Science* **290**, 1331 (2000).
10. J. Liu *et al.*, *Nature* **385**, 780 (1997).
11. M. Ahlskog *et al.*, *Chem. Phys. Lett.* **300**, 202 (1999).
12. R. Martel, H. R. Shea, P. Avouris, *Nature* **398**, 299 (1999).
13. J. Liu *et al.*, *Science* **280**, 1253 (1998).
14. J. L. Bahr, E. T. Mickelson, M. J. Bronikowski, R. E. Smalley, J. M. Tour, *Chem. Commun.* **2001**, 193 (2001).
15. A. Kuznetsova *et al.*, *Chem. Phys. Lett.* **321**, 292 (2000).
16. K. D. Ausman, R. Piner, O. Lourie, R. S. Ruoff, *J. Phys. Chem. B* **104**, 8911 (2000).
17. R. Saito, T. Takeya, T. Kimura, G. Dresselhaus, M. S. Dresselhaus, *Phys. Rev. B* **57**, 4145 (1998).
18. J. Chen *et al.*, *Science* **282**, 95 (1998).
19. P. J. Flory, *Statistical Mechanics of Chain Molecules* (Wiley, New York, 1969), pp. 401–403.
20. H. Yamakawa, W. H. Stockmayer, *J. Chem. Phys.* **57**, 2843 (1972).
21. J. Shimada, H. Yamakawa, *Macromolecules* **17**, 689 (1984).
22. J. Brandrup, E. H. Immergut, *Polymer Handbook* (Wiley, New York, ed. 3, 1989).
23. M-F. Yu, B. S. Files, S. Arepalli, R. S. Ruoff, *Phys. Rev. Lett.* **84**, 5552 (2000).
24. H. Ishida, Z. Qi, M. Sokabe, K. Donowaki, Y. Inoue, *J. Org. Chem.* **66**, 2978 (2001).

26 March 2001; accepted 12 July 2001

Atlantic Water Flow Pathways Revealed by Lead Contamination in Arctic Basin Sediments

Charles Gobeil,[1]* Robie W. Macdonald,[2] John N. Smith,[3] Luc Beaudin[1]

Contaminant lead in sediments underlying boundary currents in the Arctic Ocean provides an image of current organization and stability during the past 50 years. The sediment distributions of lead, stable lead isotope ratios, and lead-210 in the major Arctic Ocean basins reveal close coupling of the Eurasian Basin with the North Atlantic during the 20th century. They indicate that the Atlantic water boundary current in the Eurasian Basin has been a prominent pathway, that contaminant lead from the Laptev Sea supplies surface water in the transpolar drift, and that the Canadian and Eurasian basins have been historically decoupled.

The close connection between the Arctic Ocean and contaminants released to the south is well documented (*1*). Although the atmosphere can transport volatile and particulate substances into the Arctic within days, over a longer time period the oceans may become the more important pathway (*1*, *2*). Pb provides one of the clearest examples of human activities that have overwhelmed natural cycles, particularly in the North Atlantic (*3–5*). Owing to its strong affinity for particles, Pb has a short residence time in surface waters (<5 years), and contamination there is mirrored in sediments of the underlying deep basins (*6*, *7*). Because the stable Pb isotope composition varies with source, the isotopic ratios can provide an incisive indicator of pathways impacted by humans (*8*).

Here, we examine sediment cores collected from the Arctic Ocean and Greenland Sea basins for evidence of contaminant Pb. Using the contaminant Pb inventory and its isotopic composition, we infer the source of the Pb and its pathways referring to present schemes of ocean current structure and ice drift (*9*, *10*). In the abyssal ocean, where sedimentation may be less than 1 mm per thousand years and where foragers often mix the top few cm of the sediments, contaminant Pb inputs are observed as increased Pb burden in a shallow surface mixed layer (SML). With a half-life of 22.3 years, excess ^{210}Pb in the sediments, i.e., ^{210}Pb deposited from the water as opposed to that produced by ^{226}Ra decay within the sediments, is an ideal indicator of the SML where the Pb deposited over the past 100 years resides. Detection of contaminant Pb above a variable background can be considerably reinforced with stable Pb isotope compositions because contaminant Pb usually differs from natural Pb (*8*), and the isotopic composition is little affected by kinetic processes occurring between source and sink. To identify contaminant Pb in Arctic basin sediments that accumulate slowly (*11*), we use three rigorous criteria: (i) There must be a SML enriched in ^{210}Pb. (ii) The concentration of Pb must be higher in the SML than in the sediments below. (iii) The stable Pb isotope composition must differ between the SML and the deeper sediments.

Sediment box cores were collected in 1994 at depths of 2265 to 4230 m in the Canadian, Eurasian, and Greenland Sea basins (Fig. 1); they were sectioned into 1-cm slices for the top 10 cm and then analyzed. All cores exhibit well-defined SMLs in the top 2 to 4 cm on the basis of the ^{210}Pb profiles (Fig. 1). In the Eurasian Basin, Pb concentrations in the SML are 1.6 to 4.8 μg g^{-1} higher than in the sediments immediately below, and the stable isotope ratios are lower. At stations 39 and 37, the shift in the isotopic composition associated with the change in Pb concentration in the SML is larger than at stations 36 and 35. In the Canadian Basin sediments, elevated ^{210}Pb activities in surface sediments are similar to those observed in the Greenland Sea and Eurasian basins, confirming an active scavenging of ^{210}Pb from the water column. However, at stations 26 and 11, Pb concentration does not differ between the SML and the sediments immediately below, and the stable Pb isotope ratios remain invariant

---

[1] Institut Maurice-Lamontagne, Mont-Joli, QC, G5H 3Z4, Canada. [2] Institute of Ocean Sciences, Sidney, BC, V8L 4B2, Canada. [3] Bedford Institute of Oceanography, Dartmouth, NS, B2Y 4A2, Canada.

*To whom correspondence should be addressed. E-mail: GobeilC@dfo-mpo.gc.ca

(Fig. 1). At station 18, there is evidence of a slightly increased Pb concentration in the SML accompanied by a very small change in the isotopic composition. The ^{210}Pb and Pb observations together imply that contaminant Pb is almost absent from the Canadian Basin because of a lack of supply rather than an ineffectual vertical transport pathway.

For the Greenland Sea and Eurasian Basin sediment cores, the contaminant Pb inventories, calculated assuming a sediment density of 2.5 g cm^{-3} and with the measured porosity and the Pb concentration just below the SML as a background value, are 0.6, 2.5, 3.2, and 4.4 μg cm^{-2} at stations 36, 35, 37, and 39, respectively. These inventories are comparable to those reported by Hamelin *et al.* (*7*) for the Hatteras and Bermuda abyssal plains in the North Atlantic (2.8 to 4.3 μg cm^{-2}) and well exceed the atmospherically derived Pb inventory of ~0.2 μg cm^{-2} observed at the Greenland ice cap (*12*, *13*). Considering the low atmospheric flux of Pb to the Arctic in general (*13*, *14*), our sediment core data imply a surprisingly efficient delivery of contaminant Pb by ocean currents to these polar basins. Extrapolation of the results to the entire Eurasian Basin (~1.5 × 10^6 km^2) yields a total accumulation of 9 to 48 Mt of anthropogenic Pb in basin sediments.

By means of a simple two-component linear model, the isotopic composition of the contaminant Pb can be determined at stations where the stable Pb isotope ratios show the greatest changes (Fig. 2). Assuming that the fraction of natural Pb is F_N, the fraction of anthropogenic Pb is F_A, the measured Pb concentration is $\mathrm{Pb_{Meas}}$, and, for a given ratio such as ^{206}Pb/^{207}Pb, the measured value is $(^{206}\mathrm{Pb}/^{207}\mathrm{Pb})_{\mathrm{Meas}}$; then, $F_A + F_N = 1$ and $F_A\,(^{206}\mathrm{Pb}/^{207}\mathrm{Pb})_A + F_N\,(^{206}\mathrm{Pb}/^{207}\mathrm{Pb})_N = (^{206}\mathrm{Pb}/^{207}\mathrm{Pb})_{\mathrm{Meas}}$. Analogous equations apply to the other measured ratios. Isotopic compositions for natural and anthropogenic Pb were assigned after a close examination of all our isotopic data plotted as the various ratios shown in Fig. 2. The natural Pb isotopic ratios were estimated from the measurements below the SML. Ratios for anthropogenic Pb (Table 1) were assigned as follows. A range of ratio values was input to the equations, and the respective solutions for F_N and F_A, together with $\mathrm{Pb_{Meas}}$, were used to calculate the concentration of both natural and anthropogenic Pb. The best solution was constrained to that which (i) produced a natural Pb profile approximately constant with depth, (ii) yielded concentrations above zero for anthropogenic Pb in the SML only, and (iii) gave similar Pb concentrations, within the errors of measurements, when calculated with any of the Pb isotope ratios. For this latter calculation, the best fit was arrived at by minimizing the standard deviation for the Pb concentrations found with the three ratios.

The best algebraic solutions for Pb isotopic composition (shaded rectangles in Fig. 2) reflect the composite values for contaminant or natural Pb deposited into the SML over time measured in centuries. The anthropo-

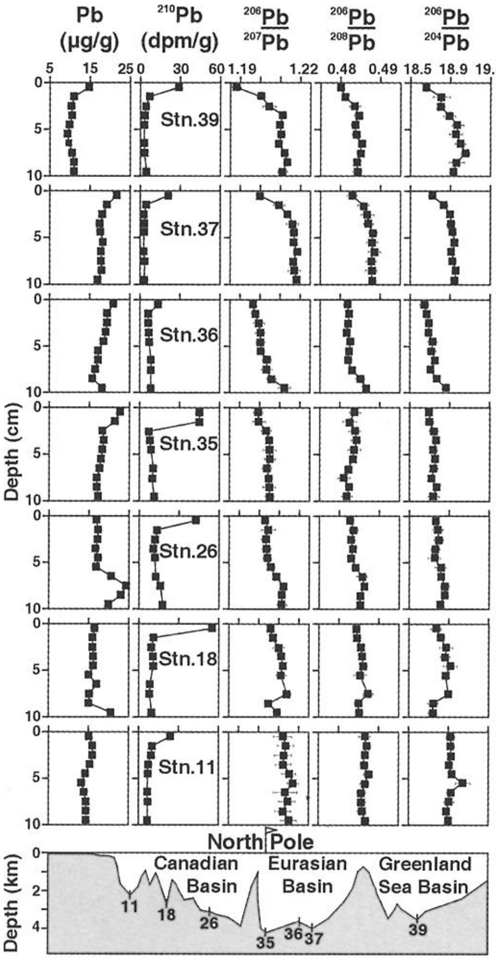

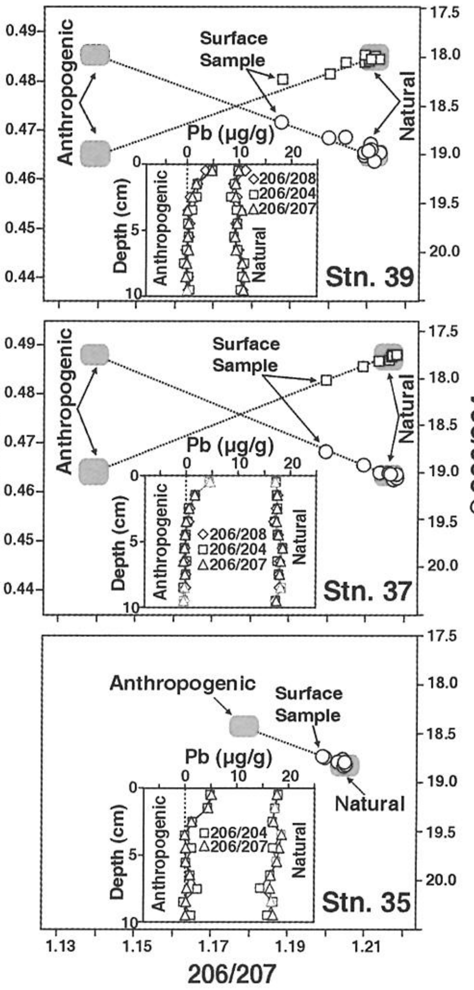

Fig. 1 (left). Depth profiles of Pb concentration, ^{210}Pb activity, and stable Pb isotope ratios (^{206}Pb/^{207}Pb, ^{206}Pb/^{208}Pb, and ^{206}Pb/^{204}Pb) in the top 10 cm of sediment cores collected in the Greenland Sea Basin (station 39), the Eurasian Basin (stations 37, 36, and 35), and the Canadian Basin (stations 26, 18, and 11). Sediment aliquots were leached during 12 hours at room temperature with 10 ml of a 1 M nitric acid solution (*25*). The concentration of Pb and its isotopic composition were then determined with an inductively coupled plasma mass spectrometer (*26*). The precision and accuracy of the Pb concentration measurements determined through repeated (n = 10) analysis of the reference sediments BEST-1 were 1 and 1.4%, respectively. Measurement errors on the stable Pb isotope ratios were typically 0.2%. The accuracy of the mass spectrometer was monitored continuously during the isotopes ratio determinations by including measurements of the Pb isotope standard SRM981. Corrections for mass fractionation were applied on every two samples. ^{210}Pb activity was determined in acid-dissolved sediment samples by alpha counting of ^{210}Po electrodeposited onto nickel disks, and the ^{226}Ra activity (assumed to represent supported ^{210}Pb) was determined by gamma spectrometry on dried sediments with an ultralow-background Ge-well detector. **Fig. 2 (right).** Plots of the ^{206}Pb/^{208}Pb (open squares) and ^{206}Pb/^{204}Pb (open circles) ratios versus ^{206}Pb/^{207}Pb ratio at stations 39, 37, and 35. The shaded rectangles represent the average isotope ratios for anthropogenic and natural Pb in the SML. These ratios were used to determine the concentration of both anthropogenic and natural Pb at each site. Similar results were obtained with each of the Pb isotope ratios.

genic Pb ratio, therefore, is an average for all contaminant Pb, most of which has been deposited during the past 70 years (*13*). The isotopic composition for anthropogenic Pb at stations 37 and 39 falls into the range typical for recent Western European sources, as summarized by Véron and Church (*15*). Specifically, the $^{206}Pb/^{207}Pb$ ratio at these stations (1.139) is within the range of the values reported for Pb aerosols in France and Germany (1.12 to 1.15) and Great Britain and Spain (1.10 to 1.13) that are heavily influenced by the low ratios (1.06 to 1.09) typical of Western European gasoline emissions (*16*). The ratio also matches the values for Western Europe (1.130 to 1.155) reported by Hopper *et al.* (*17*) and suggested (1.112 to 1.152) by Alleman *et al.* (*5*). At the North Pole (station 35), however, the calculated isotopic ratio for anthropogenic Pb is not the 1.139 found at stations 37 and 39 but rather ~1.179 (Fig. 2). Another Pb source is implied by this ratio, most likely coal combustion and industrial sources in the former USSR and Eastern Europe (*17*, *18*). Although a small increase in Pb concentration is detected in the sediment SML at stations 36 and 18, the signal is too weak to assign the isotopic composition with confidence.

A compelling story of Pb transport emerges when the sediment data are viewed in the context of Atlantic water circulation (Fig. 3) proposed by Rudels *et al.* (*9*). The relatively low Pb inventories in Western Arctic basins and contrasting high inventories at station 39 in the Greenland Sea and station 37 within the Eurasian Basin, together with the contaminant Pb isotopic composition, reveal the delivery of contaminant Pb to the Arctic Ocean in a fashion reminiscent of the radionuclides discharged to the sea from European nuclear fuel reprocessing plants (*19*). Anthropogenic lead is carried into the Arctic Ocean via both Fram Strait Branch Water (FSBW) and Barents Sea Branch Water (BSBW). Pb in BSBW is likely to have been largely scavenged from the water while it flows across the highly productive, particle-rich Barents Sea shelf whereas a much lower quantity of Pb is removed from FSBW during its passage along the continental margin of the Greenland and Norwegian seas and Nansen Basin. BSBW is cooled and freshened over the shelf with its density and depth range being expanded (to a depth of about 1300 m) as it exits the Barents Sea via the Santa Anna Trough and displaces FSBW outward (toward the interior of the Eurasian Basin). The eastward continuation of Atlantic water flowing in a boundary current around the southern end of the Nansen Basin and across the Lomonosov Ridge into the Western Arctic Ocean contains 50 to 80% BSBW (*20*), whereas water that recirculates in the Eurasian Basin has a proportionally greater component of FSBW. With BSBW having been largely stripped of its anthropogenic Pb, both over the shelf and during its 5- to 10-year transit around the continental margin, there is little residual signal available for deposition in the Western Arctic basins. In contrast, sediments in the Nansen Basin (e.g., stations 36 and 37) are subject to Pb contamination by direct scavenging from FSBW during its initial passage along the continental margin or by nephloid transport of contaminated sediments from shelf/slope regimes. The different isotopic composition of contaminant Pb at the North Pole (station 35) suggests that replenishment of contaminant Pb has occurred from Eastern European/Russian sources, probably via the Eastern Laptev Sea (*10*).

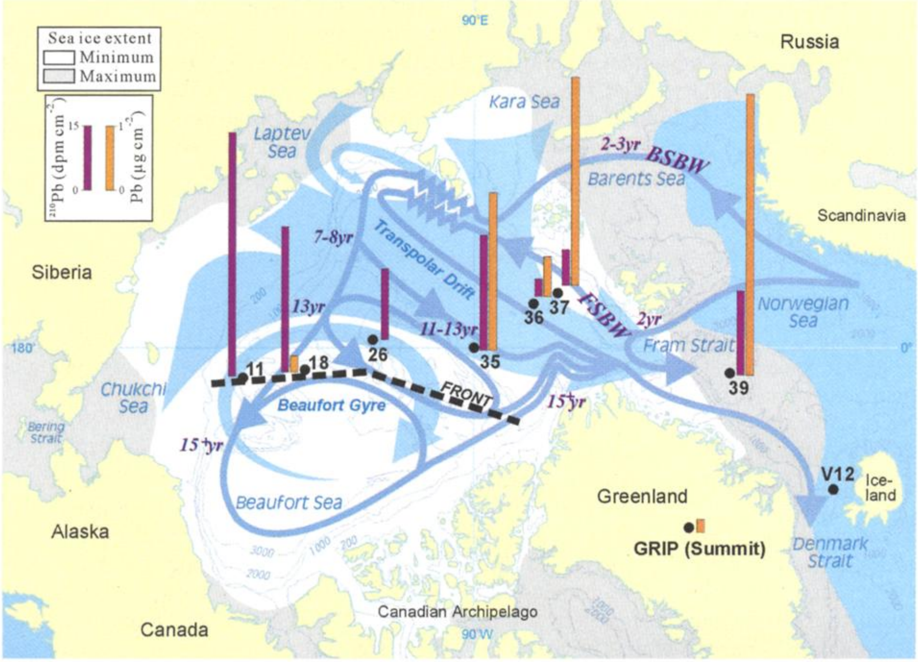

Fig. 3. Inventories of contaminant Pb (orange bars) and excess ^{210}Pb (red bars, calculated as the difference between the total ^{210}Pb activity illustrated in Fig. 1 and the background ^{226}Ra activity for each core). The boundary currents of Atlantic water (blue arrows) proposed by Rudels *et al.* (*9*) provide a simple transport mechanism to explain the distribution of contaminant Pb within the Eurasian Basin sediments; the low inventory observed at the Greenland ice cap (*13*) suggests the atmosphere to be a minor pathway. The times of transit from the North Sea (blue italics) [as described by Smith *et al.* (*27*) and Smethie *et al.* (*28*)] and the Pb isotopic composition (not shown) suggest that contaminant Pb deposited at stations 39 and 37 derives from Western Europe whereas Pb at station 35 derives from Eastern Europe/Russia, probably via the Eastern Laptev Sea (*10*). There is no evidence of contaminant Pb in Canadian Basin sediments except for the small signal observed at station 18 under the continuation of the Atlantic water boundary current. The ^{210}Pb inventories show that Pb is scavenged relatively effectively from the water column, implying that lack of contaminant Pb in Canadian Basin sediment is due to a lack of supply of contaminant Pb to the water. The recent location of the front between Atlantic and Pacific surface water masses (dashed line) is drawn from Morison *et al.* (*29*). GRIP (Summit), Greenland Ice Core Project Summit.

Table 1. Pb isotope ratios for anthropogenic Pb in the SML at stations 39, 37, and 35. Numbers in parenthesis represent SD.

Station	$^{206}Pb/^{207}Pb$ (± 0.003)	$^{206}Pb/^{204}Pb$ (± 0.05)	$^{206}Pb/^{208}Pb$ (± 0.001)
39	1.139	17.98	0.4651
37	1.139	17.75	0.4642
35	1.179	18.38	–

Although ice efficiently transports particles (*21*) and must therefore carry particulate Pb from the Laptev Sea across the North Pole (Fig. 3), we cannot tell whether it is the ice or the water in the transpolar drift that provides the more important pathway to the pole sediments. It is possible that ice transports most of its burden to the Greenland Sea, where it is deposited when the ice melts. The continuation of the transpolar drift in the East Greenland current passes near a station just north of Iceland (station V12, Fig. 3), where Véron *et al.* (*22*) determined a $^{206}Pb/^{207}Pb$ ratio of 1.165 to 1.178 in surface water. This value is close to our determination for contaminant Pb at the North Pole (∼1.179), lies within the range of Eastern European sources, and could signify the export of Pb from the Laptev Sea either in ice or water—a process that takes as little as 2 years (*23*). Finally, the Pb data suggest that the recent displacement of the front between the Atlantic and Pacific water masses into the Canadian Basin (Fig. 3) is unusual in that contaminant Pb, which may be transported there from the Laptev Sea under the present circulation regime (*24*), is simply not evident.

References and Notes

1. R. W. Macdonald *et al.*, *Sci. Total Environ.* **254**, 93 (2000).
2. J. N. Smith, K. M. Ellis, L. R. Kilius, *Deep Sea Res. Part I* **45**, 959 (1998).
3. B. K. Schaule, C. C. Patterson, in *Trace Elements in Seawater*, C. S. Wong *et al.*, Eds. (Plenum, New York, 1983), pp. 487–504.
4. E. A. Boyle, S. D. Chapnick, G. T. Shen, M. P. Bacon, *J. Geophys. Res.* **91**, 8573 (1986).
5. L. Y. Alleman, A. J. Véron, T. M. Church, A. R. Flegal, B. Hamelin, *Geophys. Res. Lett.* **26**, 1477 (1999).
6. A. Véron, C. E. Lambert, A. Isley, P. Linet, F. Grousset, *Nature* **326**, 278 (1987).
7. B. Hamelin, F. Grousset, E. R. Sholkovitz, *Geochim. Cosmochim. Acta* **54**, 37 (1990).
8. C. C. Patterson, D. M. Settle, *Mar. Chem.* **22**, 137 (1987).
9. B. Rudels, E. P. Jones, L. G. Anderson, G. Katner, in *The Polar Oceans and Their Role in Shaping the Global Environment*, vol. 85 of *Geophysical Monograph Series*, O. M. Johannessen, R. D. Muench, J. E. Overland, Eds. (American Geophysical Union, Washington, DC, 1994), pp. 33–46.
10. F. Schoster, M. Behrends, C. Müller, R. Stein, M. Wahsner, *Int. J. Earth Sci.* **89**, 486 (2000).
11. D. A. Darby, J. F. Bishof, G. A. Jones, *Deep Sea Res. Part II* **44**, 1745 (1997).
12. M. Murozumi, T. J. Chow, C. C. Patterson, *Geochim. Cosmochim. Acta* **33**, 1247 (1969).
13. S. Hong, J.-P. Candelone, C. C. Patterson, C. F. Boutron, *Science* **265**, 1841 (1994).
14. F. A. Akeredolu *et al.*, *Atmos. Environ.* **28**, 1557 (1994).
15. A. J. Véron, T. M. Church, *J. Geophys. Res.* **102**, 28049 (1997).
16. F. Monna, J. Lancelot, I. W. Croudace, A. B. Cundy, J. T. Lewis, *Environ. Sci. Technol.* **31**, 2277 (1997).
17. J. F. Hopper, H. B. Ross, W. T. Sturges, L. A. Barrie, *Tellus* **43B**, 45 (1991).
18. W. T. Sturges, J. F. Hopper, L. A. Barrie, R. C. Schnell, *Atmos. Environ.* **27A**, 2865 (1993).
19. H. D. Livingston, *Philos. Trans. R. Soc.* **25**, 161 (1988).
20. U. Schauer *et al.*, *Ann. Geophys.*, in press.
21. H. Eicken *et al.*, *Geophys. Res. Lett.*, **27**, 1919 (2000).
22. A. J. Véron, T. M. Church, I. Rivera-Duarte, A. R. Flegal, *Deep Sea Res. Part II* **46**, 919 (1999).
23. I. Rigor, *ARCOS Newsl.* **44**, 1 (1992).
24. A. Y. Proshutinsky, M. A. Johnson, *J. Geophys. Res.* **102**, 12493 (1997).
25. A. Ng, C. C. Patterson, *Geochim. Cosmochim. Acta* **46**, 2307 (1982).
26. Y. Erel, Y. Dubowski, L. Halicz, J. Erez, A. Kaufman, *Environ. Sci. Technol.* **35**, 292 (2001).
27. J. N. Smith, K. M. Ellis, T. M. Boyd, *J. Geophys. Res.* **104**, 29663 (1999).
28. W. M. Smethie Jr., P. Schlosser, T. S. Hopkins, G. Boenisch, *J. Geophys. Res.* **105**, 1105 (2000).
29. J. Morison, M. Steele, R. Andersen, *Deep Sea Res. Part I* **45**, 15 (1998).

30. Copyright, Her Majesty in right of Canada, as represented by the Minister of Fisheries and Oceans.

31. We thank R. Shearer and D. Stone for the Canadian Northern Contaminants Program; the U.S. Office of Naval Research for funding support (J.N.S.); and D. Paton for technical assistance at sea.

2 May 2001; accepted 2 July 2001

Southward Migration of the Intertropical Convergence Zone Through the Holocene

Gerald H. Haug,[1] Konrad A. Hughen,[2] Daniel M. Sigman,[3] Larry C. Peterson,[4] Ursula Röhl[5]

Titanium and iron concentration data from the anoxic Cariaco Basin, off the Venezuelan coast, can be used to infer variations in the hydrological cycle over northern South America during the past 14,000 years with subdecadal resolution. Following a dry Younger Dryas, a period of increased precipitation and riverine discharge occurred during the Holocene "thermal maximum." Since ∼5400 years ago, a trend toward drier conditions is evident from the data, with high-amplitude fluctuations and precipitation minima during the time interval 3800 to 2800 years ago and during the "Little Ice Age." These regional changes in precipitation are best explained by shifts in the mean latitude of the Atlantic Intertropical Convergence Zone (ITCZ), potentially driven by Pacific-based climate variability. The Cariaco Basin record exhibits strong correlations with climate records from distant regions, including the high-latitude Northern Hemisphere, providing evidence for global teleconnections among regional climates.

The Cariaco Basin, an anoxic marine basin on the northern shelf of Venezuela, is a highly sensitive recorder of past climates in the tropical ocean (*1–4*), in part because its position causes it to accumulate sediments of both marine and terrestrial origin. At ∼10°N, the basin sits at the northern edge of the annual latitudinal range of the ITCZ, with the ITCZ nearly overhead during the summer. During this season, rain falls in regions that drain directly into the Cariaco Basin or that contribute to flow in the Orinoco River (*5*). The subsequent runoff transports terrigenous materials to the coast and offshore, where they accumulate in sediments of the Cariaco Basin and surrounding shelf (*3*). During the winter/spring, when the ITCZ is located over the equator or further south, local river runoff is diminished, and the northeast trade winds shift south and intensify over the Cariaco Basin (*5*). These strong winds drive upwelling along the Venezuelan coast that feeds biological production in Cariaco surface waters, delivering organic matter and calcareous and siliceous microfossils to the seafloor. This seasonal alternation between river runoff and upwelling is recorded in the lamination of the Cariaco sediments, with dark-colored terrigenous grain-rich layers deposited during the rainy summer/fall and lighter-colored biogenic-rich layers deposited during the windy winter/spring (Fig. 1). The absence of oxygen in deep basin waters prevents bioturbation, resulting in a continuous, largely laminated sediment sequence spanning the last 14.5 thousand years (ky) (*1, 2*).

Ocean Drilling Program (ODP) Site 1002 (10°42.73′N, 65°10.18′W) was drilled at a water depth of 893 m (*6*), well below the depth (∼300 m) at which oxygen-free conditions in the Cariaco water column currently begin. We report on the uppermost 5.5 m of the 170-m sediment sequence recovered at Hole 1002C, which covers the last 14 ky. The laminated nature of the sediments and the high deposition rates (∼30 cm/ky) in this natural sediment trap yield an important tropical counterpart to high-latitude ice cores for the study of climate change at interannual to millennial time scales. Detailed age control is based on a series of 10 accelerator mass spectrometry (AMS) ^{14}C dates of the planktic foraminifer *Globigerina bulloides*, all transferred to calendar years using the calibration of (*7*).

Bulk sedimentary iron (Fe) and titanium (Ti) were measured over this interval at 2 mm spacing, corresponding to a sampling interval of ∼4 to 5 years, with a profiling x-ray fluorescence scanner at the University of Bremen (Figs. 2 and 3) (*8*). This represents the maximum resolution of this new instrument. In our 14-ky-long record, Ti and Fe concentrations were generally low in sediments deposited during the Younger Dryas cold period between 12.6 and 11.5 thousand years ago (ka). Their concentrations increased during the "Preboreal" period (11.5 to 10.5 ka) and were

---

[1] Department of Earth Sciences, Eidgenössische Technische Hochschule–Zentrum, CH-8092 Zürich, Switzerland. [2] Woods Hole Oceanographic Institution, Woods Hole, MA 02543, USA. [3] Department of Geosciences, Princeton University, Princeton, NJ 08544, USA. [4] Rosenstiel School of Marine and Atmospheric Science, University of Miami, Miami, FL 33149, USA. [5] Fachbereich Geowissenschaften, Universität Bremen, D-28334 Bremen, Germany.